Critical Population Density Triggers Rapid Formation of Vast Oceanic Fish Shoals

Nicholas C. Makris,[1]* Purnima Ratilal,[2] Srinivasan Jagannathan,[1] Zheng Gong,[2] Mark Andrews,[2] Ioannis Bertsatos,[1] Olav Rune Godø,[3] Redwood W. Nero,[4] J. Michael Jech[5]

Similarities in the behavior of diverse animal species that form large groups have motivated attempts to establish general principles governing animal group behavior. It has been difficult, however, to make quantitative measurements of the temporal and spatial behavior of extensive animal groups in the wild, such as bird flocks, fish shoals, and locust swarms. By quantifying the formation processes of vast oceanic fish shoals during spawning, we show that (i) a rapid transition from disordered to highly synchronized behavior occurs as population density reaches a critical value; (ii) organized group migration occurs after this transition; and (iii) small sets of leaders significantly influence the actions of much larger groups. Each of these findings confirms general theoretical predictions believed to apply in nature irrespective of animal species.

Many species of oceanic fish band together in large shoals (*1*, *2*) that can span tens of kilometers and involve hundreds of millions of individuals. Grouping leads to survival advantages through enhanced spawning, predator avoidance, and feeding mechanisms (*3*–*6*). Little information has been available about the formation process and behavior of large oceanic fish shoals. Traditional methods rely on local measurements from slow-moving research vessels that enable sampling of only a small fraction of a shoal during an entire survey, typically by vertical profiling, and cannot distinguish between temporal and spatial changes (*7*–*9*). Here, we describe fundamental temporal and spatial processes by which vast oceanic shoals form by observation of entire shoals in space and time over their full horizontal extent and relate these processes to likely governing mechanisms. We do this using Ocean Acoustic Waveguide Remote Sensing (OAWRS) (*10*), which enables instantaneous imaging and continuous monitoring of oceanic fish populations over tens of thousands of square kilometers.

We studied *Clupea harengus* (Atlantic herring), because they are known to regularly mass in large shoals for spawning at specific times and locations like other clupeid fish. Clupeids are keystone species in many of the world's major marine ecosystems, from the coastal upwelling regions of South America and Africa to the temperate areas of the Nordic Sea, Baltic Sea, and Gulf of Maine (*11*). They provide trophic links between plankton, such as krill, and larger predators, such as humans, birds, whales, dolphins, seals, sharks, cod, pollock, and haddock (*12*). Georges Bank is one of the primary spawning grounds for herring in the Gulf of Maine, which was once one of the world's most productive fisheries before its collapse in the 1970s (*8*, *13*). Herring migrate to Georges Bank to spawn in early autumn, typically September and October, from offshore regions of the Gulf of Maine and beyond (*8*, *14*).

We used OAWRS to monitor herring behavior continuously on Georges Bank during the autumn 2006 spawning season, in conjunction with traditional conventional fish-finding sonar (CFFS) (*9*) and trawl (*8*) line transects. The OAWRS system instantaneously imaged areas spanning 100 km in diameter every 75 s and so enabled continuous time-space monitoring of shoaling behavior over an ecosystem scale. We focused our experiment on regions where herring shoals were most likely to form. We determined these regions by analysis of a decade of National Marine Fisheries Services (NMFS) annual surveys made with conventional line-transect methods. These historic data showed that the herring traditionally first mass in dense layers near the seafloor along the northern flank of Georges Bank in deeper water (150 to 200 m) before spawning just to the south in shallow waters on the bank (<50 m).

We found shoal formation to depend on initial conditions and to ensue rapidly when these conditions were satisfied. First, we found that the preexisting population density of diffusely scattered individuals had to reach a critical threshold of 0.2 fish per square meter (fish/m^2). Given this, we found shoal formation to consistently commence in a highly organized fashion near sunset, apparently triggered by reduction in light level. The process depended on orderly and coherent horizontal convergences of leading individuals to produce denser and thicker vertical layers at a few discrete horizontal locations. This process occurred within favored bathymetric contours (Fig. 1). From preexisting diffuse background levels consistent with scattered individuals displaying no coherent interaction (Fig. 1A), small catalyzing clusters of much higher areal population density emerge in OAWRS imagery within the favored bathymetric contours (160 to 190 m) just before sunset (Fig. 1B), introducing bursts of coherent horizontal structure. Simultaneous vertical profiles from CFFS line transects show that, before the leading clusters form, the fish are widely distributed in a diffuse low-density layer within 5 m of the seafloor (Fig. 2A). The leading clusters (100-m horizontal scale) form as thick (10 to 30 m in the vertical) and dense groups within 20 to 40 m of the seafloor (Fig. 2A), when the fish rise slightly and converge in the horizontal as seen in both OAWRS (Fig. 1, A and B) and CFFS data (Fig. 2A). Formation of these denser clusters requires horizontal convergence by conservation of mass from the original thin, low-density layers.

The emergence of leading clusters of high population density set off chain reactions that caused rapid growth into vast shoals. We found the growth to propagate horizontally outward as convergence waves emanating from the cluster initiation points, which appeared to act as sources of the wave action. The waves propagated over tens of kilometers in tens of minutes, as can be seen for example in Fig. 1, A to F, and Fig. 3. The 3.0 to 6.0 m/s propagation speed of these waves (Fig. 3A) is an order of magnitude faster than the typical 0.2 m/s speed at which herring swim (*15*) and so is likely the apparent speed (*10*) of sequences of local synchronous convergence actions and reactions (*16*, *17*) by members of the shoal. Such local actions define a propagating compressional wave in a medium of variable density (*18*). Our observations provide experimental evidence for the existence of compressional waves in vast fish shoals, which have been predicted in physical theories (*19*). We found these shoal-forming waves to be highly directional and to propagate most rapidly along the direction of favored bathymetric contours (Fig. 1, A to F). Before the waves appeared, areal population density slowly increased at a rate of 0.06 to 0.1 fish/m^2 per hour (Fig. 3, B and C). As soon as the critical density of 0.2 fish/m^2 was reached (Fig. 3, B and C), coherent shoal-forming waves appeared (Fig. 3A), and the population density rapidly increased at a rate of roughly 5 fish/m^2 per hour (Fig. 3, B and C).

After formation, we observed growth in shoal width and population as light levels remained low in the evening. Growth normal to the favored bathymetric contours appeared to be from movement of surrounding diffusely scattered fish populations to the shoal, which acted as an attractor (Fig. 1, G to L). These vast shoals, sometimes extending continuously for 40 km (Fig. 1I), would remain stable throughout the evening and dissipate as light levels increased with sunrise. When viewed vertically with CFFS transects, the shoals evolved from small, isolated, catalyzing clusters (Fig. 2A) to extensive, dense layers within 20 to 40 m of the sea floor, but typically disconnected from it by a few meters (Fig. 2B). The layer growth required horizontal convergence by conservation of fish mass.

Once vast shoals formed, they migrated at speeds consistent with the synchronous swimming of hundreds of millions of individual fish, in accord with the predictions of general behavioral models. The migrations, however, were not in a random direction, as in some theoretical models (*19*–*21*), but toward southern spawning grounds on Georges Bank, apparently for synchronized reproductive activities. Such a migration of the 3 October shoal's southern edge, from near the alpha-to-omega CFFS

[1]Massachusetts Institute of Technology, 77 Massachusetts Avenue, Cambridge, MA 02139, USA. [2]Northeastern University, 360 Huntington Avenue, Boston, MA 02115, USA. [3]Institute of Marine Research, Post Office Box 1870, Nordnes, N-5817 Bergen, Norway. [4]Southeast Fisheries Science Center, 3209 Frederic Street, Pascagoula, MS 39568, USA. [5]Northeast Fisheries Science Center, 166 Water Street, Woods Hole, MA 02543, USA.

*To whom correspondence should be addressed. E-mail: makris@mit.edu

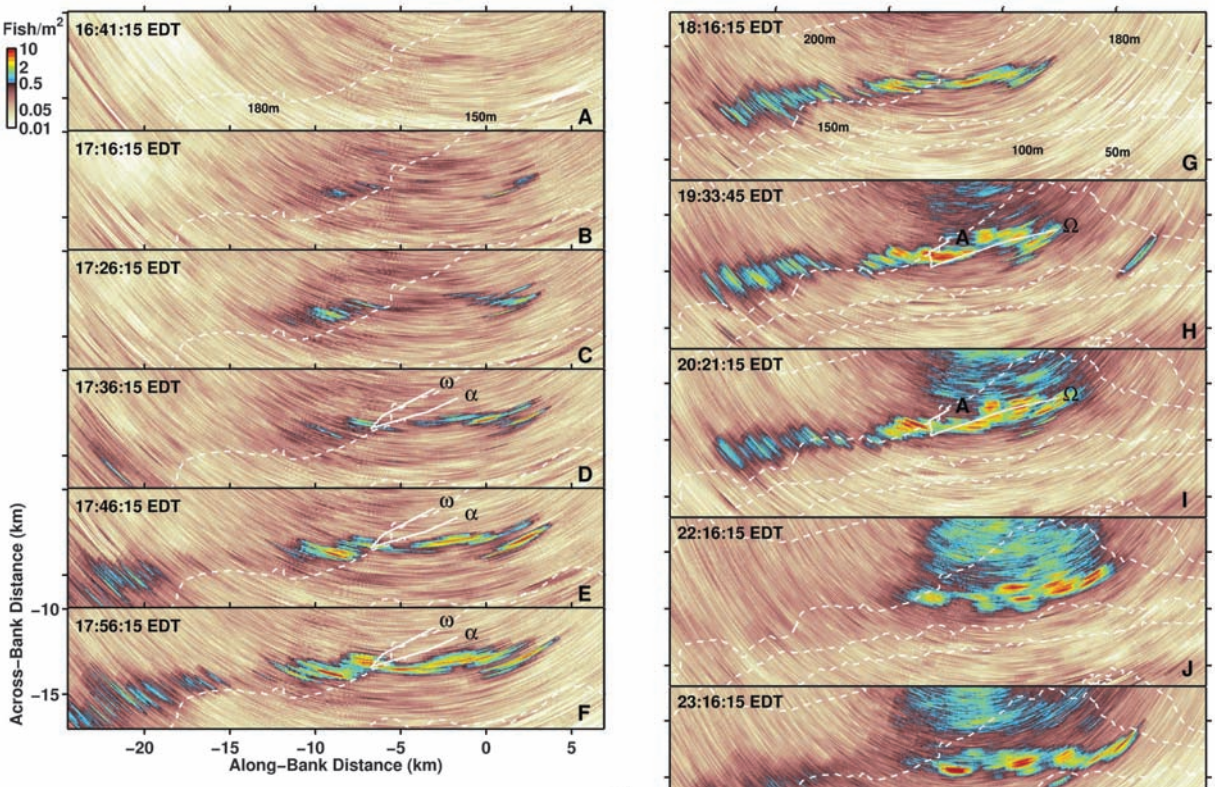

Fig. 1. Millions of Atlantic herring abruptly form vast shoals on 3 October 2006 just before sunset, which was at 18:08 EDT, on the northern flank of Georges Bank. (**A** to **F**) Sequence of instantaneous OAWRS areal density (fish/m^2) images illustrating initiation and along-bank shoal growth over tens of kilometers in tens of minutes. (**G** to **L**) Spatial and temporal evolution of massive herring shoals during the evening of 3 October 2006. Instantaneous OAWRS images taken over 6 hours illustrate shoal thickening in the across-bank direction and gradual migration of its southern edge. Roughly 250 million herring (50,000 tons) are imaged in (L), or 5 to 20% of the entire Georges Bank stock based on NMFS CFFS line-transect surveys (Fig. 4E) and combined CFFS, bottom trawls, and catch landings (*12*). Our simultaneous capture trawl surveys show that over 99% of the fish imaged by OAWRS within the dense shoals are Atlantic herring, combined with a small fraction of Acadian redfish (*Sebastes fasciatus*) and haddock (*Melanogrammus aeglefinus*). The moored OAWRS source is the coordinate origin in all OAWRS images, at 42.2089°N, 67.6892°W on 3 October. The positive vertical axis in all OAWRS images points 16° counter-clockwise of true north. The dashed lines indicate water depth contours.

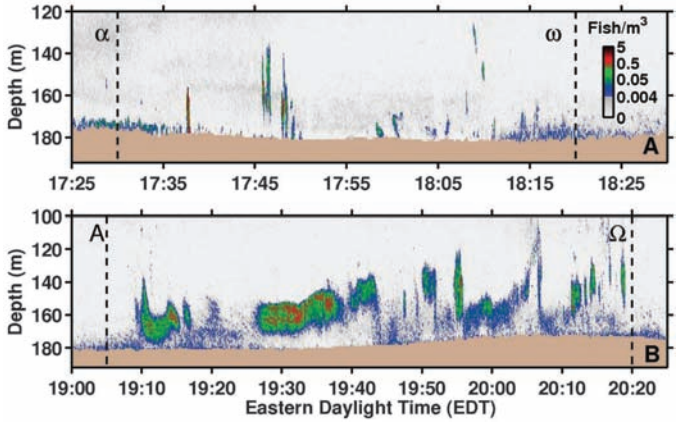

Fig. 2. Time-depth profile of fish volumetric density (fish/m^3) measured by CFFS along: (**A**) the V-shaped line transect shown in Fig. 1, D to F, and (**B**) the J-shaped line transect through the shoal shown in Fig. 1, H and I. Black dashed vertical lines correspond to transect start (alpha) and end (omega) points.

transect of Fig. 1H to the 150-m contour 2 to 4 km to the south in Fig. 1L, is evident in the most populous region and quantified in Fig. 3A. The migration is slow, roughly 0.2 m/s (Fig. 3A), which is consistent with the average swimming speed of herring in a school (*15*). Another example of a southern migration appears in Fig. 4 for 29 September. Shoals first form as usual by sunset (Fig. 4, A and B). Massive portions of their southern edges then migrate upslope from depths greater than 50 m (Fig. 4B) to spawning grounds 2 to 3 km to the south where depths are less than 50 m (Fig. 4D). The migration speed is similar to that observed on 3 October, following that expected for the material displacement of millions of swimming herring. Dense evening shoals sometimes developed a diffuse northern component (Fig. 1, H to L), which could indicate a north-south migration route for spawning herring from offshore regions of the Gulf of Maine to Georges Bank. The southern edge of the shoals, in contrast, was typically sharp (Fig. 1, G to L), following the general bathymetric contour of the spawning grounds of Georges Bank, indicating the leading edge of a synchronous mass migration.

We found the overall process of rapid shoal formation, triggered by attainment of a critical density of 0.2 fish/m^2 near sunset, and subsequent migration toward spawning grounds to define a regular diurnal behavioral pattern that was consistently observed (*22*) during our roughly 1-week measurement period as shown in Figs. 1 to 4 and Figs. S1 to S4. The

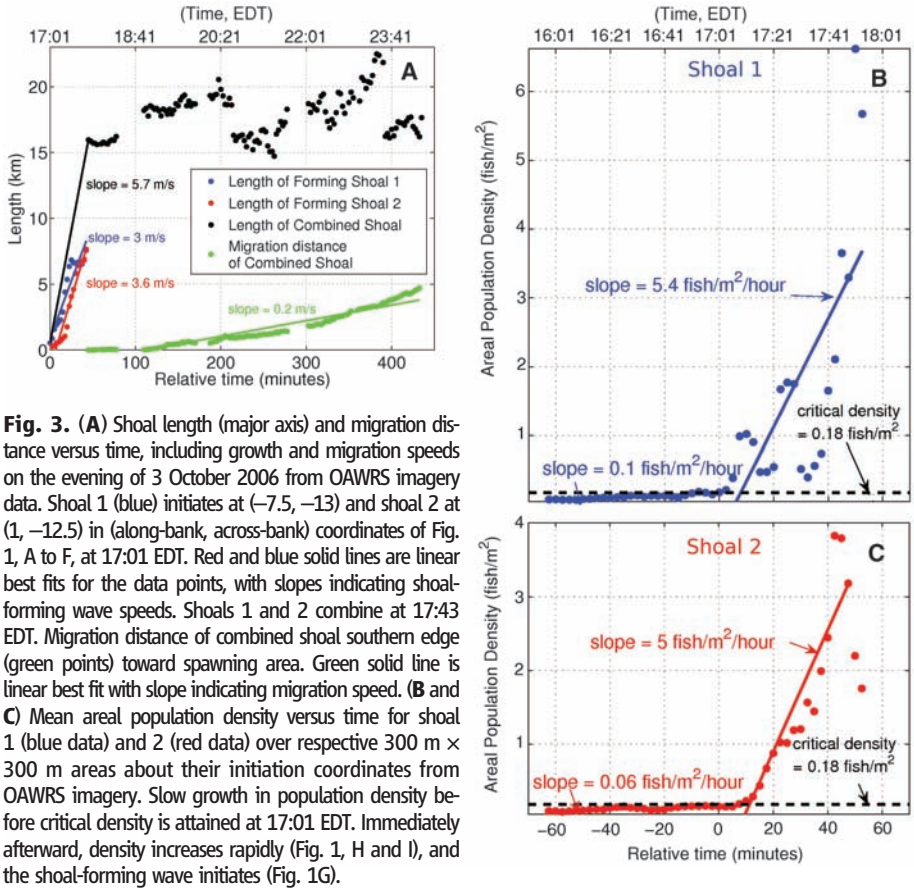

Fig. 3. (**A**) Shoal length (major axis) and migration distance versus time, including growth and migration speeds on the evening of 3 October 2006 from OAWRS imagery data. Shoal 1 (blue) initiates at (–7.5, –13) and shoal 2 at (1, –12.5) in (along-bank, across-bank) coordinates of Fig. 1, A to F, at 17:01 EDT. Red and blue solid lines are linear best fits for the data points, with slopes indicating shoal-forming wave speeds. Shoals 1 and 2 combine at 17:43 EDT. Migration distance of combined shoal southern edge (green points) toward spawning area. Green solid line is linear best fit with slope indicating migration speed. (**B** and **C**) Mean areal population density versus time for shoal 1 (blue data) and 2 (red data) over respective 300 m × 300 m areas about their initiation coordinates from OAWRS imagery. Slow growth in population density before critical density is attained at 17:01 EDT. Immediately afterward, density increases rapidly (Fig. 1, H and I), and the shoal-forming wave initiates (Fig. 1G).

evidence suggests the primary biological function of the shoals is a prelude to synchronized spawning. Close proximity of individuals can induce synchronous reproductive development through visual and olfactory stimulus (*17*). Synchronous development is often critical because each female must typically produce a large number of eggs within very tight time constraints to enable group spawning (*17*, *23*). Shoal formation at greater depths allows these activities to proceed with reduced risk of attack from predators (*24*), such as pilot whales, porpoise, and tuna, that prefer to hunt in the shallower spawning grounds (*4*, *25*). Evening formation allows matching and subsequent migration to spawning grounds to occur under cover of darkness, with more safety from predator attack. The shoaling behavior we observed is evidently unrelated to diurnal feeding (*4*) activities, because trawl samples obtained during our survey show 99% of the herring have empty stomachs and have not yet spawned. This is consistent with historic observations showing that herring do not feed during the spawning period (*26*).

More generally, our observations during the spawning period show the formation processes of large oceanic fish shoals (i) require initial conditions on population density and external stimuli, such as light level; (ii) follow the actions of a small number of leaders; (iii) rely upon extremely rapid and efficient time-space convergence events that propagate as coherent waves over great distances by chain reaction; and (iv) involve extensive horizontal structures that evolve in a highly organized and predictable

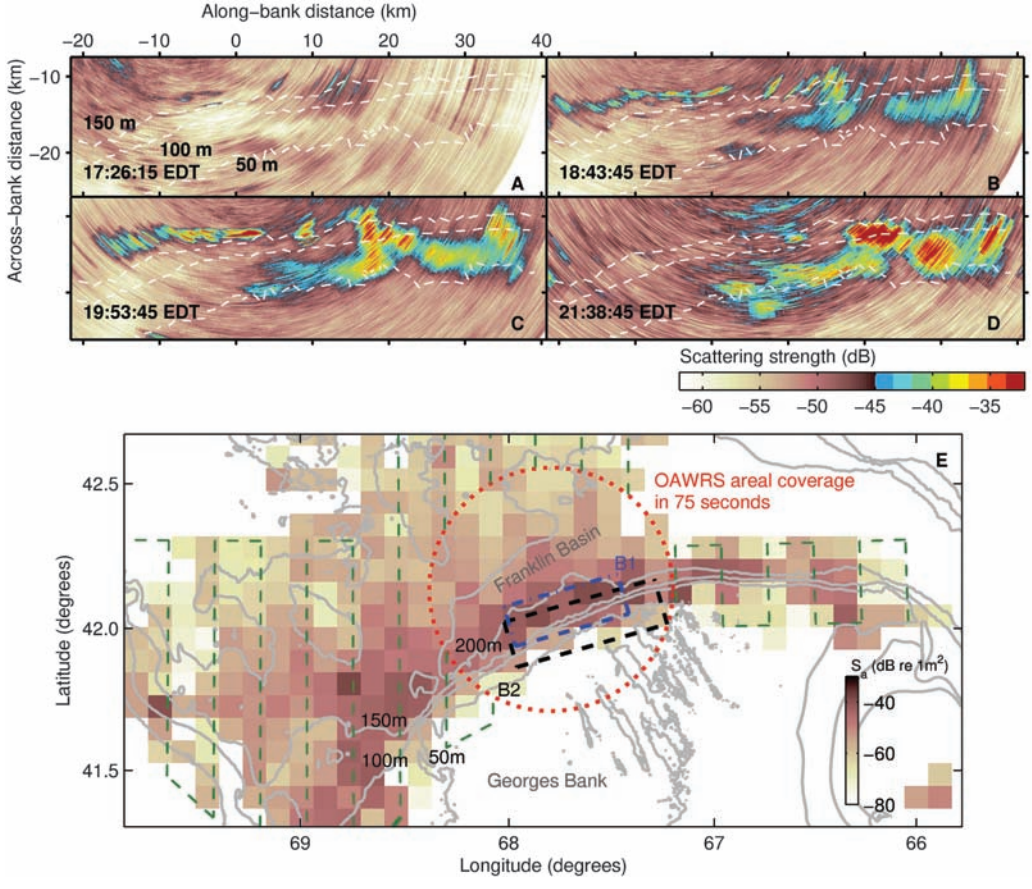

Fig. 4. (**A** to **D**) Sequence of OAWRS scattering strength (*32*) images illustrates formation, growth, and subsequent southern migration of herring shoals toward the Georges Bank spawning grounds on the evening of 29 September 2006. Sunset was at 18:15 EDT. Same region as Fig. 1, G to L. (**E**) Backscattering strength s_a (*33*) at 5 by 5 nautical miles (1 nmi = 1852 m) grid obtained by averaging CFFS line-transect data from 1999 through 2005 NMFS Annual Fall Herring Surveys (*34*). Boxes B1 and B2 are regions shown in Fig. 1, G to L, and Fig. 4, A to D, respectively. Regions of maximum herring concentration are consistent between OAWRS 2006 imagery (Fig. 1) and NMFS 6-year average (Fig. 4E). Red circle indicates OAWRS areal coverage in 75 s. Green dashed line indicates the line transect of a typical 2-week NMFS survey, not shown within red circle.

manner. The rapidity with which these shoal-forming waves spread once the initial conditions are satisfied is indicative of the advantage the group has over the isolated individual in transferring information over great distances. Our observations also provide ecosystem-scale evidence that a critical population density triggers rapid transition from disordered to highly synchronized behavior, and small groups of leaders often play crucial roles in affecting the actions of much larger groups, as has recently been predicted in general theoretical investigations (*19*, *21*, *27*–*29*), simulations, and laboratory experiments (*26*, *27*) about animal group behavior (*20*, *30*, *31*). These findings provide information essential to the conservation of marine ecosystems that vast oceanic fish shoals inhabit.

References and Notes

1. J. H. S. Blaxter, J. R. Hunter, *Adv. Mar. Biol.* **20**, 1 (1982).
2. D. J. Hoare, G. D. Ruxton, J.-G. J. Godin, J. Krause, *Oikos* **89**, 546 (2000).
3. T. J. Pitcher, J. K. Parrish, in *The Behaviour of Teleost Fishes*, T. J. Pitcher, Ed. (Chapman & Hall, London, 1993), pp. 363–439.
4. M. Milinski, in *Predation Risk and Feeding Behaviour*, T. J. Pitcher, Ed. (Chapman & Hall, London, 1993), pp. 285–305.
5. D. P. Croft, J. Krause, I. D. Couzin, T. J. Pitcher, *Fish Fish.* **4**, 138 (2003).
6. T. J. Pitcher, in *Encyclopedia of Ocean Sciences*, J. H. Steele, K. K. Turekian, S. A. Thorpe, Eds. (Academic Press, London, 2001), pp. 978–987.
7. O. R. Godø *et al.*, *ICES J. Mar. Sci.* **61**, 1093 (2004).
8. W. J. Overholtz, J. M. Jech, L. Michaels, L. D. Jacobson, P. J. Sullivan, *J. Northwest Atl. Fish. Sci.* **36**, 127 (2006).
9. D. N. MacLennan, E. J. Simmonds, *Fisheries Acoustics* (Chapman & Hall, London, 1992).
10. N. C. Makris *et al.*, *Science* **311**, 660 (2006).
11. C. Ray, C. R. Robins, J. Douglass, R. T. Peterson, *Peterson Field Guide: Atlantic Coast Fishes* (Houghton Mifflin, New York, 1999).
12. W. J. Overholtz, J. S. Link, *ICES J. Mar. Sci.* **64**, 83 (2007).
13. W. J. Overholtz, *Fish. Res.* **57**, 237 (2002).
14. V. N. Zinkevich, *ICNAF Bull.* **4**, 101 (1967).
15. I. Huse, E. Ona, *ICES J. Mar. Sci.* **53**, 863 (1996).
16. L. Nottestad *et al.*, *Sarsia* **80**, 277 (1996).
17. G. Skaret, L. Nottestad, A. Ferno, A. Johannessen, B. E. Axelsen, *Aquat. Living Resour.* **16**, 299 (2003).
18. J. W. S. Rayleigh, in *The Theory of Sound*, J. W. S. Rayleigh, R. B. Lindsay, Eds. (Dover, New York, 1976), vol. 2, pp. 1–48.
19. J. Toner, Y. Tu, *Phys. Rev. E* **58**, 4828 (1998).
20. G. Gregoire, H. Chate, *Phys. Rev. Lett.* **92**, 025702 (2004).
21. T. Vicsek, A. Czirok, E. Ben-Jacob, I. Cohen, O. Schochet, *Phys. Rev. Lett.* **75**, 1226 (1995).
22. Materials and methods are available as supporting material on *Science* Online.
23. R. Vabo, G. Skaret, *Ecol. Modell.* **214**, 125 (2008).
24. S. Mackinson, *J. Fish Biol.* **55**, 972 (1999).
25. R. Toresen, *ICES J. Mar. Sci.* **48**, 15 (1991).
26. J. S. Link, J. Brunett, *J. Fish Biol.* **59**, 783 (2001).
27. J. Buhl *et al.*, *Science* **312**, 1402 (2006).
28. S. G. Reebs, *Anim. Behav.* **59**, 403 (2000).
29. I. D. Couzin, J. Krause, N. R. Franks, S. Levin, *Nature* **433**, 513 (2005).
30. D. J. T. Sumpter, *Philos. Trans. R. Soc. London Ser B* **361**, 5 (2006).
31. S. V. Viscido, J. K. Parrish, D. Grunbaum, *Ecol. Modell.* **183**, 347 (2005).
32. R. J. Urick, *Principles of Underwater Sound* (McGraw-Hill, New York, 3rd ed., 1983).
33. D. N. MacLennan, P. G. Fernandes, J. Dalen, *ICES J. Mar. Sci.* **59**, 365 (2002).
34. J. M. Jech, W. L. Michaels, *Can. J. Fish. Aquat. Sci.* **63**, 2225 (2006).

35. This research was supported by the National Oceanographic Partnership Program, the Office of Naval Research, and the Alfred P. Sloan Foundation and is a contribution to the Census of Marine Life. We would like to thank the science parties, officers, and crew of the research vessels *Oceanus*, *Endeavor*, *Delaware II*, and *Hugh Sharp*.

Supporting Online Material

www.sciencemag.org/cgi/content/full/323/5922/1734/DC1
Materials and methods
Figs. S1 to S6
References
Movie S1

8 December 2008; accepted 19 February 2009
10.1126/science.1169441

Genetic Contribution to Variation in Cognitive Function: An fMRI Study in Twins

Jan Willem Koten Jr.,[1,2]* Guilherme Wood,[3] Peter Hagoort,[4,7] Rainer Goebel,[5,8] Peter Propping,[6] Klaus Willmes,[1] Dorret I. Boomsma[2]

Little is known about the genetic contribution to individual differences in neural networks subserving cognition function. In this functional magnetic resonance imaging (fMRI) twin study, we found a significant genetic influence on brain activation in neural networks supporting digit working memory tasks. Participants activating frontal-parietal networks responded faster than individuals relying more on language-related brain networks. There were genetic influences on brain activation in language-relevant brain circuits that were atypical for numerical working memory tasks as such. This suggests that differences in cognition might be related to brain activation patterns that differ qualitatively among individuals.

The direct link between genes, brain, and behavior can be difficult to establish (*1*). Structural and functional investigations in the human and mouse brain suggest that some genes are expressed in highly specific brain regions, whereas other genes have more global effects (*1*–*4*). The total heritability of individual differences can be examined with twin studies (*5*–*8*). Functional magnetic resonance imaging (fMRI) studies investigating specific brain regions assumed to subserve some cognitive function did not demonstrate high heritability of brain activity (*9*–*14*). Genetic influences on brain activation in areas that typically subserve a cognitive function might be modest because these areas will be activated similarly among humans. By contrast, brain regions activated in some individuals only might be better candidates for genetic analysis. Thus, genetic effects should be tested cortex-wide.

Structural and functional brain investigations suggest that brain areas that are similarly activated among humans may be embedded in larger brain networks that vary among individuals (*1*, *4*), possibly causing individual differences in cognition. An attractive candidate for the study of genetic influences on brain networks is working memory for digits under arithmetic distraction. Heritability estimates for behavioral measures in this task are high (*15*), and stable individual differences in the spatial organization of function-carrying areas were shown (*16*). A distractor task causes an interruption of verbal rehearsal, leading to rapid forgetting (*17*). The decay model of working memory (*18*, *19*) states that numbers can be retained without explicit verbal rehearsal, but it does not specify neural correlates of these memory processes. The triple-code model (*20*) claims that number processing and arithmetic require both magnitude and language-related number representations in inferior parietal cortex, angular gyrus, and perisylvian cortex. Individuals holding numbers in memory in a language-related or magnitude code suffer from code interference when executing arithmetic tasks. Employing early motor coding routes protects memory traces from distraction (*21*), which corresponds to the importance of finger representations for number processing also in adulthood (*22*).

For genetic fMRI studies, appropriate brain alignment, sufficient individual differences, reliability, and statistical power are of core importance (*6*, *23*–*25*). We used an extended twin design consisting of male monozygotic (MZ) twins with an additional nontwin brother, where every brother is related to both twins. We examined reaction times (RT) as a measure of proficiency and blood oxygen level–dependent (BOLD) response as a measure of relative brain (de)activation (*26*) during two identical scanning sessions in all participants. These two observations of the phenotypes of interest were entered into a genetic structural equation model (SEM) that estimates additive genetic effects corrected for measurement error (*23*). Heritability h^2 was expressed as the percentage of reliable variance accounted for

[1]Section Neuropsychology, RWTH Aachen University, Germany. [2]Biological Psychology, Vrije Universiteit, Amsterdam, Netherlands. [3]Institute of Psychology, Paris-Lodron University Salzburg, Austria. [4]Donders Institute for Brain, Cognition, and Behaviour, Radboud University Nijmegen, Netherlands. [5]Department of Cognitive Neuroscience, Faculty of Psychology, Maastricht University, Netherlands. [6]Institute of Human Genetics, University of Bonn, Germany. [7]Max Planck Institute for Psycholinguistics, Nijmegen, Netherlands. [8]Netherlands Institute for Neuroscience, an institute of the Royal Netherlands Academy of Arts and Sciences (KNAW), Amsterdam, Netherlands.

*To whom correspondence should be addressed. E-mail: jan.koten@gmx.de

Supporting Online Material for

Critical Population Density Triggers Rapid Formation of Vast Oceanic Fish Shoals

Nicholas C. Makris,* Purnima Ratilal, Srinivasan Jagannathan, Zheng Gong, Mark Andrews, Ioannis Bertsatos, Olav Rune Godø, Redwood W. Nero, J. Michael Jech

*To whom correspondence should be addressed. E-mail: makris@mit.edu

Published 27 March 2009, *Science* **323**, 1734 (2009)
DOI: 10.1126/science.1169441

This PDF file includes

Other Supporting Online Material for this manuscript includes the following:
(available at www.sciencemag.org/cgi/content/full/323/5922/1734/DC1)

Materials and Methods

The overall process of rapid shoal formation, triggered by attainment of a critical density of 0.2 fish/m^2 near sunset, followed by migration towards spawning grounds, is found to describe a regular diurnal pattern. The pattern was observed on 7 of 7 days in the central region of Georges Bank's northern flank during the herring spawning period, and defined the dominant behavior observed there. In this central region, of the highest historical spawning populations (Fig 4E), OAWRS sampling of the shoal formation process was relatively complete on 5 days, September 28, 29, October 1-3, and fragmentary on 2 days, September 30, Oct 5, due to severe autumn weather or logistical constraints at sea. The diurnal shoal formation pattern was also observed by OAWRS at the south western end of Georges Bank's northern flank on September 26, 27, but mixed with apparent eastward migrations of preexisting shoals in the daytime and at night. Later observations at this southwestern extremity on October 4 revealed little activity, suggesting the herring observed there earlier had migrated eastwards.

Documentation of the shoal formation process for the 5 days in the central region of Georges Bank's northern flank when OAWRS sampling was relatively complete appears in Figs 1-4 of the main text for October 3 and September 29, Figs S1-S4 for September 28-29 and October 1-2, and Movie S1 for October 3. Shoal forming convergence waves, traveling at speeds much greater than herring groups swim, consistently appeared near sunset when a critical density of 0.2 fish/m^2 was attained. This was followed by much slower southern migrations consistent with herring group swimming speeds, as shown in Fig 3 and Fig S1-S4. The waves originated within favored bathymetric contours (160-190 m) from small catalyzing clusters, which acted as sources, and tended to propagate along these contours. This led to the formation of large shoals which often extended for tens of kilometers along the northern flank of Georges Bank as shown in Figs 1, 4, S1-S4. The observed shoal forming waves arose from sequences of local synchronous convergence actions and reactions by members of the shoal, which define propagating compressional waves in a medium of variable density (*S1*). Such waves have been theoretically predicted to exist in large animal groups (*S2*). Compressional waves in fish shoals require the propagation of changes in population density and so are inherently different from turning waves (*S3*) which only require the propagation of changes in fish orientation. Our observations show that a small group of leaders initiated shoal formation. Since migration typically occurred sometime after the shoals had already developed, it is not clear that the same leaders responsible for shoal initiation were also responsible for choosing a migration direction. The fact that all migrations were directed towards the spawning ground, however, indicates that the shoal migration directions were not random but were strongly influenced by synchronous spawning behavior.

Population density versus time as shown in Figs 3B-C, S1D-F, S2D, S3B, S4D-E, is the spatial average over a 0.6 km by 0.6 km patch around the region where the shoal initiates in OAWRS imagery. The two solid lines in these figures, whose slopes indicate the rate of change of population density before and after the transition, are the linear least square fits to data points they span. The slopes before a critical density of 0.2 fish/m^2 is attained are consistently orders of magnitude smaller than those after it is attained. Intersection of these least square lines before and after the transition consistently occurs at 0.2 fish/m^2 when rounded to the nearest tenth. The shoal lengths of Figs 3A, S1C, S2C, S3A, S4C, were determined from OAWRS imagery by finding the major axis extent of population density features exceeding 0.2 fish/m^2. The migration distances of southern shoal edges were determined by segmenting the shoal edges with a 0.2 fish/m^2 threshold and estimating the mean location of this edge for a given shoal from OAWRS imagery. The lines shown for shoals lengths during formation and migration distances are linear least square fits to the data points of corresponding color.

Our autumn 2006 OAWRS experiment in the Gulf of Maine and Georges Bank employed four research vessels, the RV Oceanus which towed the OAWRS receiving array and collected OAWRS data, the RV Endeavor from which the OAWRS source array was deployed in either moored or drift mode, the RV Hugh Sharp which collected CFFS data, and the RV Delaware II which collected CFFS and trawl data. The RV Delaware II also conducted the National Marine Fisheries Service Annual Fall Herring Survey

with traditional methods for measuring the distribution, abundance and behavior of oceanic fish populations (*S4*-*S7*). The beamwidth of the CFFS used by RV Hugh Sharp in our field experiment was 7.0° at 38 kHz, which yields a 20 m diameter resolution footprint at 160-m depth where many of the fish groups we imaged were concentrated, while that for the RV Delaware II was 12.0° at 38 kHz (Fig 2A-B) which leads to a 33 m diameter resolution footprint at 160-m depth.

We used the same OAWRS imaging system described in Ref (*S8*) for all OAWRS measurements presented here, which are the scattered returns of linear frequency modulated (LFM) source waveform transmissions of 50 Hz bandwidth and 1 second duration centered at 950 Hz. Scattered returns at the receiver were beamformed and match filtered leading to a range resolution of 15 m. OAWRS azimuthal resolution in radians varies as the acoustic wavelength λ (1.55 m) divided by the projected array length $L\cos\theta$, where L is the full array length (47.25 m) and the azimuth angle θ is zero at *broadside*, which is normal to the array axis. While 1 second transmissions were sent every 75 seconds at various non-overlapping frequencies to enable imaging over a 100 km diameter, consecutive LFM transmissions centered at 950 Hz were typically sent only every 150 seconds. All OAWRS images presented here are the averaged returns of 3 consecutive 950 Hz LFM transmissions and two consecutive 15-m range cells to obtain intensity averaged with at least 6 independent samples at each pixel of 30-m dimension. Scattering strength (*S9*) was obtained by correcting the measured beamformed and match filtered pressure level for transmitted level, array beampattern and two-way transmission loss (*S10*, *S11*) which was determined by parabolic equation modeling (*S8*, *S11*). OAWRS incident signals were at least 3 orders of magnitude less intense than those of the CFFS. Population density was estimated from scattering strength by determining the mean fish scattering cross section at the OAWRS frequency necessary for OAWRS and CFFS population densities to match over regions where simultaneous measurements of statistically stationary fish populations were available (*S8*).

An example of the measured pressure level of scattered returns after beamforming and match filtering appears in Fig S5A, which is the same data as that presented in Fig 1G before conversion to fish population density. The lack of apparent speckle noise fluctuations in these images is a result of (i) our standard 6-sample intensity average, and (ii) inherent variance reduction from application of the matched filter to fluctuating signals received in an ocean waveguide (*S11*). The mean measured pressure level along the transect shown in Fig S5A appears in Fig S5B with experimentally determined standard deviations for our standard 6-sample (3-ping and 2-range-cell) intensity average. These measured standard deviations range from 1.1 to 1.6 dB as shown in Fig S5B or 29% to 45% of our standard 6-sample-averaged OAWRS intensity data. These measured standard deviations are consistent with the theory and previous measurements of received circular complex Gaussian field data (*S8*, *S12*-*S16*) after matched filtering and intensity averaging (*S11*). The expected two-way transmission loss (TL) along the Fig S5A transect is shown in Fig S5C, determined from parabolic equation based Monte Carlo modeling with measured bathymetry and oceanography. It is dominated by the two-way cylindrical spreading loss of a waveguide and has small variation over the depths where fish shoals were observed by CFFS (Fig 2). The mean two way TL trend is consistent with that of our measured pressure level in Figs S5B where large fish shoals are not found, i.e. ranges other than 9.5-13 km. Statistical analysis of our experimental data shows that the stationary averaging we employed leads to a standard deviation per pixel in the OAWRS population density estimates presented of roughly 1-2 dB in regions where shoal populations follow a stationary random process in space and time consistent with that determined by the simultaneous CFFS measurements needed to determine the expected fish scattering cross-section at OAWRS frequencies. This standard deviation is due to the combined effects of received field fluctuation from transmission, scattering, and source level calibration. We were not able to convert scattering strength to fish population density for the fish groups observed in regions shallower than the 100-m bathymetric contour due to lack of corresponding CFFS measurements of fish depth distributions and population densities in those regions. Fig 4A-D is left in terms of scattering strength because much of the population observed has migrated to depths shallower than 100 m.

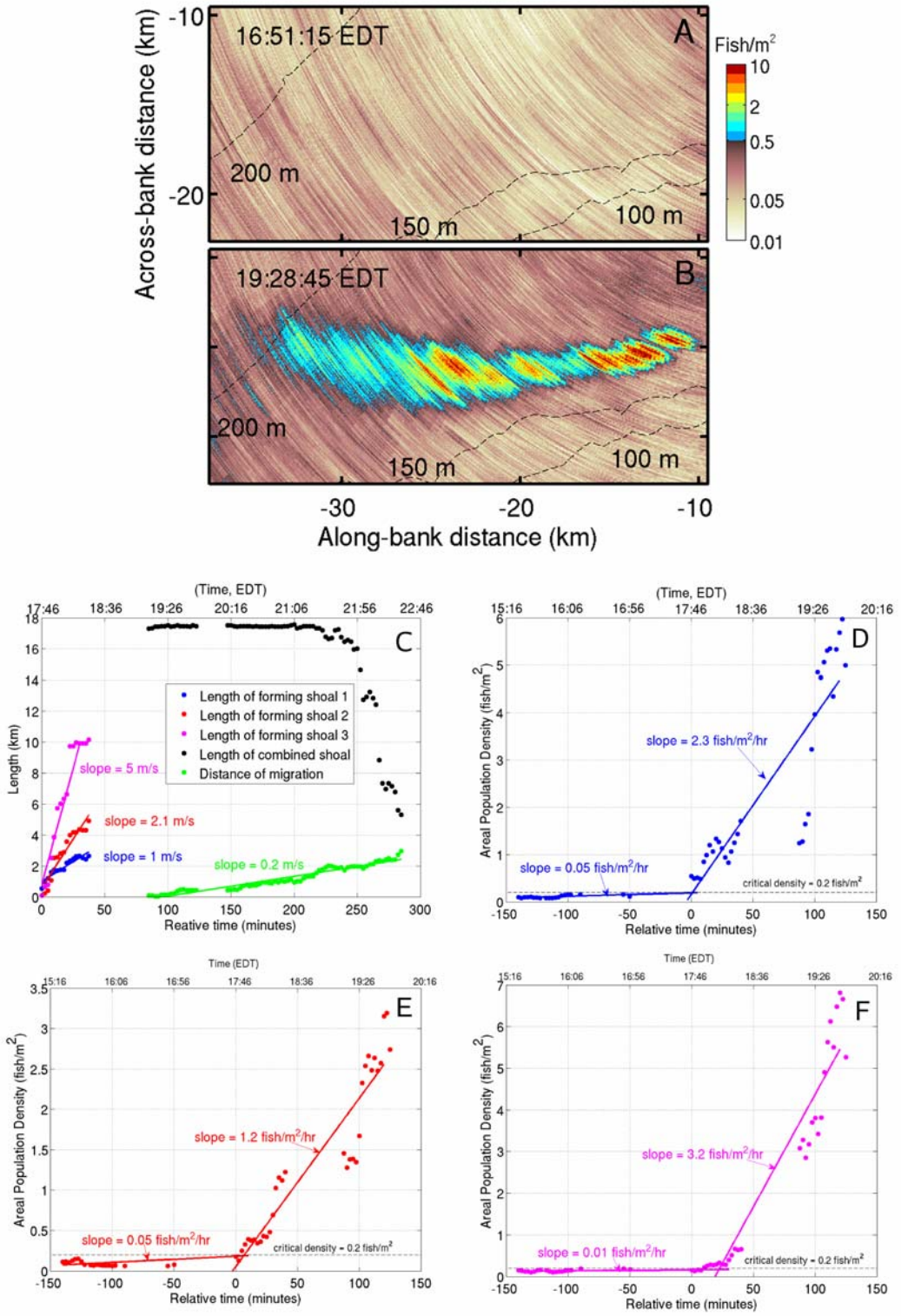

Fig S1. (A-B) OAWRS areal density (fish/m^2) on 2 Oct. 2006 illustrates shoal emergence near sunset, which was at 18:10 EDT. The origin of the coordinate system is at the source location 42.2089°N, 67.6892°W. Spatial location of region imaged is shown in Fig S6. (C) Shoal length (major axis) and migration distance versus time, including growth and migration speeds on the evening of Oct 2, 2006 from OAWRS imagery data. Shoal 1 (blue) initiates at (-12,-15), Shoal 2 (red) at (-27,-16) and Shoal 3 (magenta) at (-19,-16) in (along-bank, across-bank) coordinates of Fig S1A-B at 17:46 EDT. Magenta, red and blue solid lines are linear best fits for the data points, with slopes indicating shoal forming wave speeds. Shoals 1, 2 and 3 combine between 18:30 EDT and 19:00 EDT. Migration distance of combined shoal southern edge (green points) towards spawning area. Green solid line is linear best fit with slope indicating migration speed. (D-F) Mean areal population density versus time for Shoal 1 (blue data), 2 (red data) and 3 (magenta data) over respective 600 m x 600 m areas about their initiation coordinates from OAWRS imagery. Slow growth in population density before critical density is attained at 17:46 EDT. Immediately afterward density increases rapidly and shoal forming wave initiates.

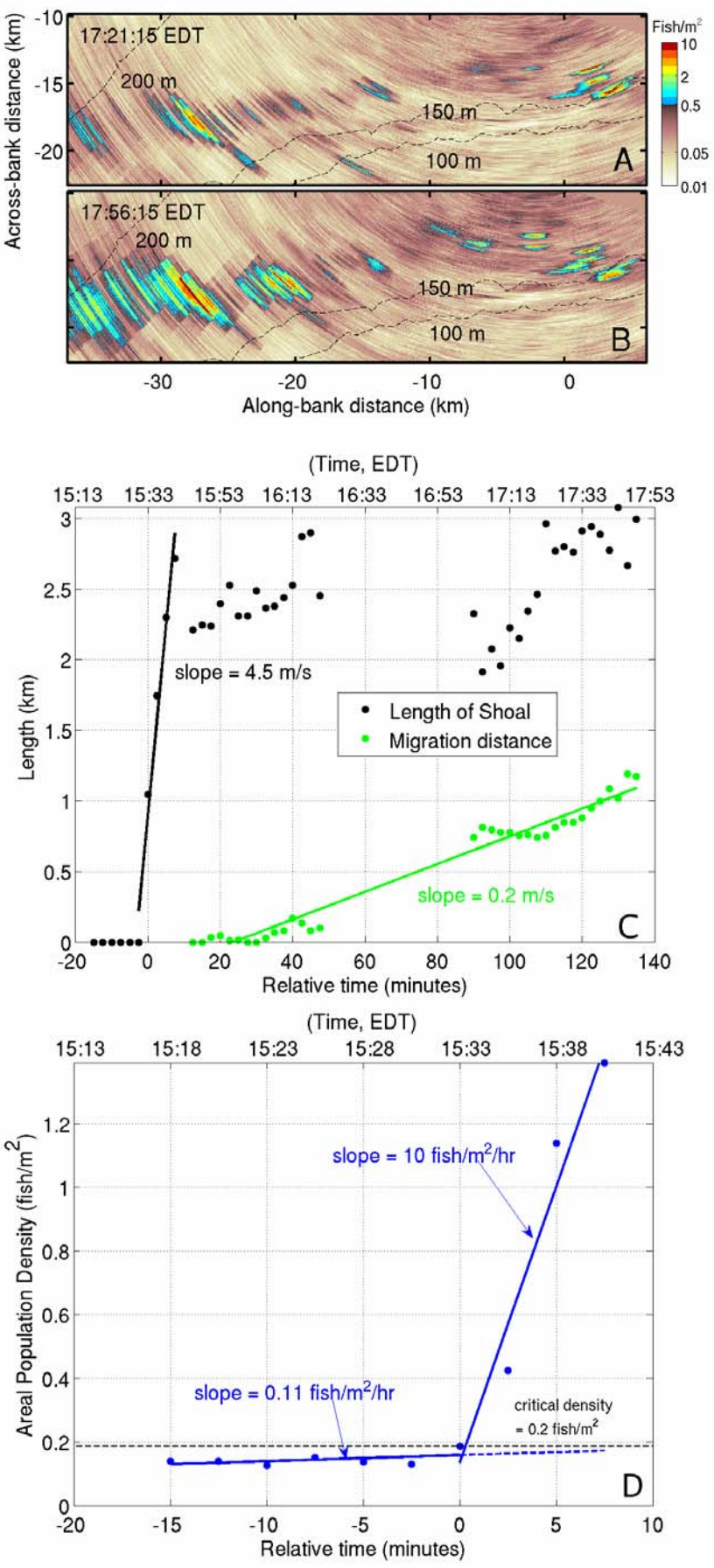

Fig S2. (A-B) OAWRS areal density (fish/m^2) on 1 Oct. 2006 illustrates sparse shoal emergence near sunset, which was at 18:11 EDT. The origin of the coordinate system is at the source location 42.2089°N, 67.6892°W. (C) Shoal length (major axis) and migration distance versus time, including growth and migration speeds on the evening of Oct. 1, 2006 from OAWRS imagery data. Shoal initiates at (2,-12) in (along-bank, across-bank) coordinates of Fig S2A-B at 15:33 EDT. Black solid line is linear best fit for the data points with slope indicating shoal forming wave speed. Migration distance of the shoal's southern edge (green points) towards spawning area. Green solid line is linear best fit with slope indicating migration speed. (D) Mean areal population density of the shoal versus time over a 600 m x 600 m area about its initiation coordinates from OAWRS imagery. Slow growth in population density before critical density is attained at 15:33 EDT. Immediately afterward density increases rapidly and shoal forming wave initiates.

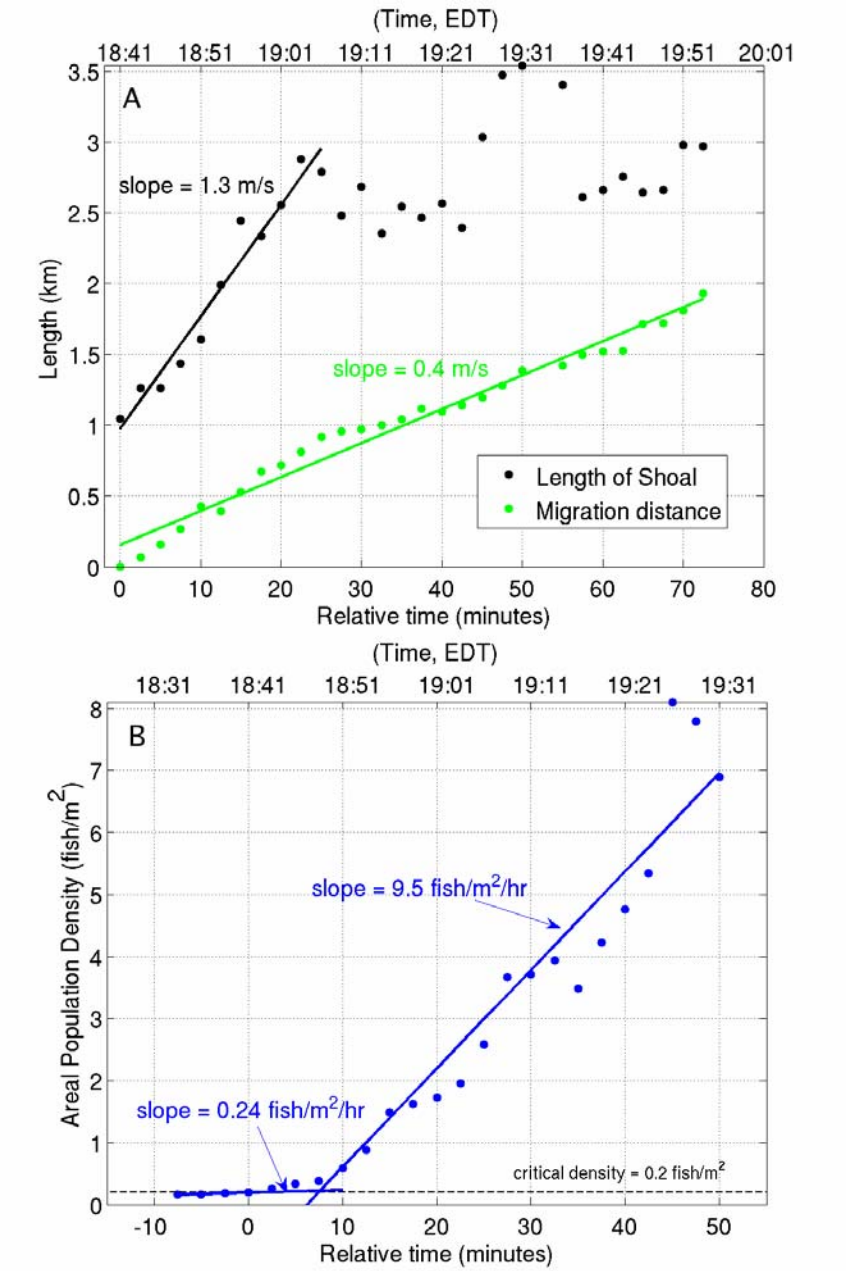

Fig S3. (A) Shoal length (major axis) and migration distance versus time, including growth and migration speeds on the evening of Sept. 29, 2006 from OAWRS imagery data. Shoal initiation was missed due to a data gap. An already initiated shoal of 1 km length passes through (5,-12) in (along-bank, across-bank) coordinates of Fig 4A-D at zero relative time and continues to grow. Black solid line is linear best fit for the data points with slope indicating shoal forming wave speed. Migration distance of the shoal's southern edge (green points) towards spawning area. Green solid line is linear best fit with slope indicating migration speed. (B) Mean areal population density of the shoal versus time over a 600 m x 600 m area about its southern edge. Slow growth in population density before critical density is attained at 18:51 EDT. Immediately afterward density increases rapidly as shoal forming wave propagates through.

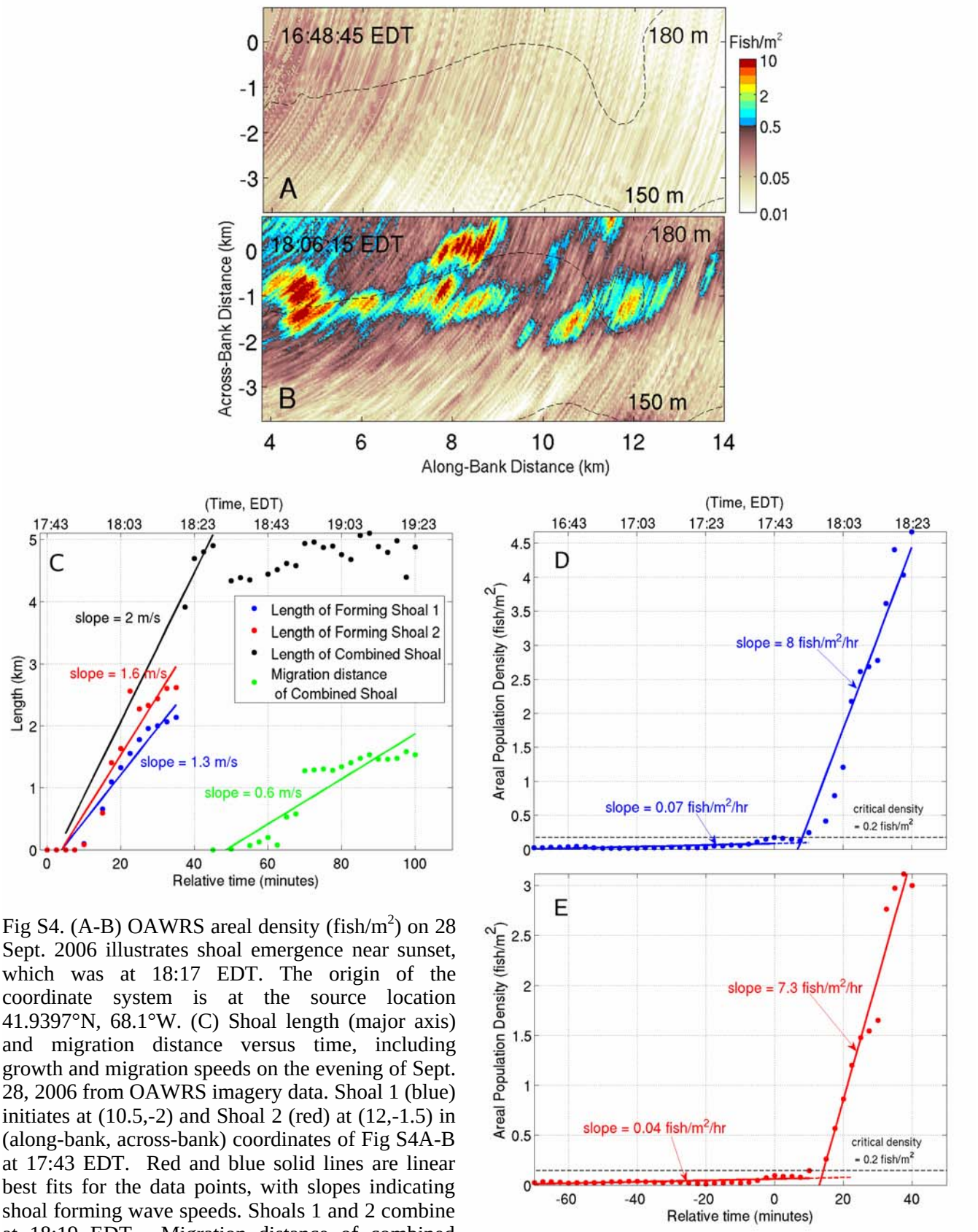

Fig S4. (A-B) OAWRS areal density (fish/m^2) on 28 Sept. 2006 illustrates shoal emergence near sunset, which was at 18:17 EDT. The origin of the coordinate system is at the source location 41.9397°N, 68.1°W. (C) Shoal length (major axis) and migration distance versus time, including growth and migration speeds on the evening of Sept. 28, 2006 from OAWRS imagery data. Shoal 1 (blue) initiates at (10.5,-2) and Shoal 2 (red) at (12,-1.5) in (along-bank, across-bank) coordinates of Fig S4A-B at 17:43 EDT. Red and blue solid lines are linear best fits for the data points, with slopes indicating shoal forming wave speeds. Shoals 1 and 2 combine at 18:19 EDT. Migration distance of combined shoal southern edge (green points) towards spawning area. Green solid line is linear best fit with slope indicating migration speed. (D-E) Mean areal population density versus time for Shoal 1 (blue data) and 2 (red data) over respective 600 m x 600 m areas about their initiation coordinates from OAWRS imagery. Slow growth in population density before critical density is attained at 17:43 EDT. Immediately afterward density increases rapidly and shoal forming wave initiates.

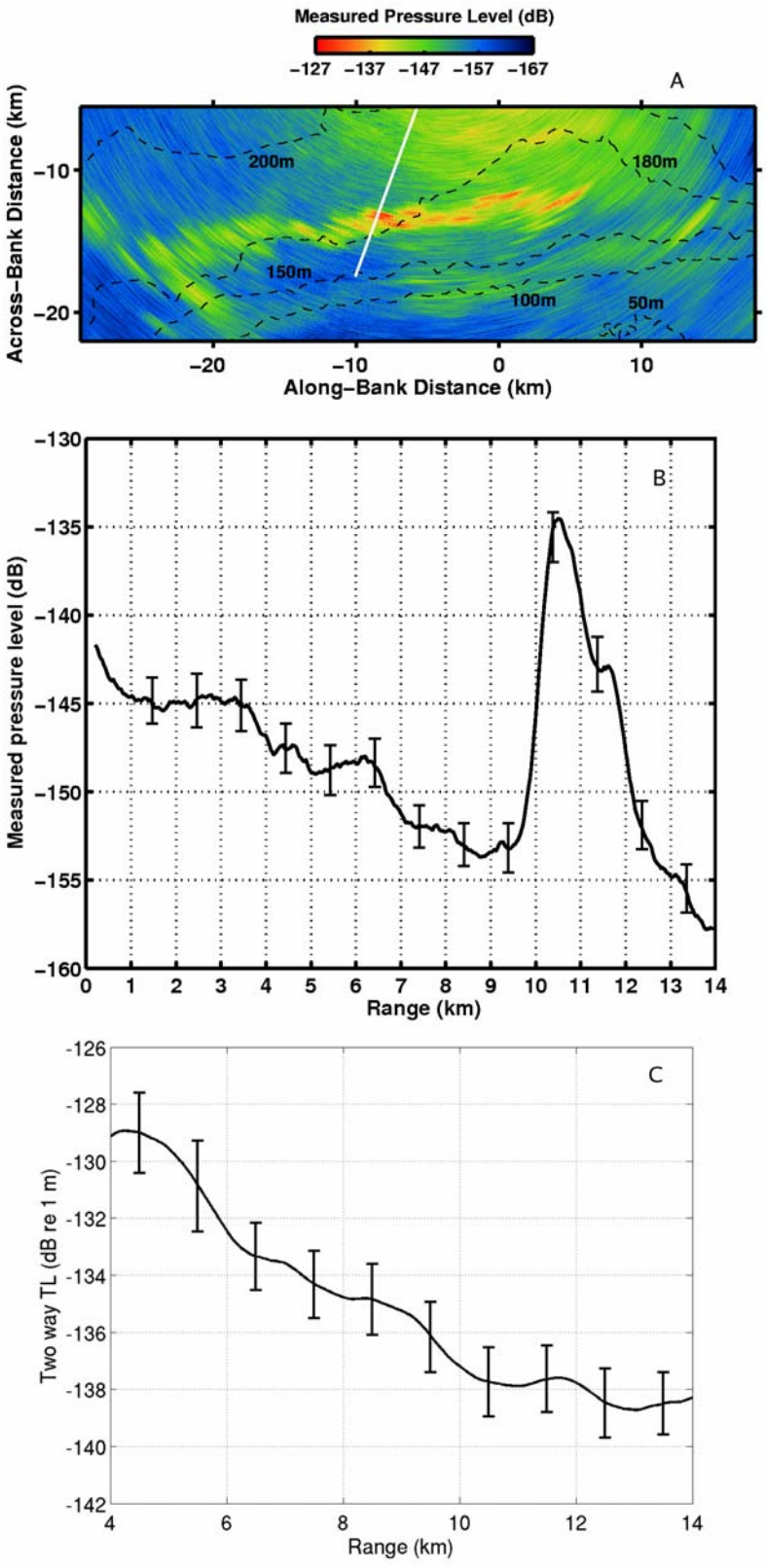

Fig S5. (A) Measured pressure level of scattered returns after beamforming and match filtering in dB re 1 m, normalized to unit source power. Same data as that presented in Fig 1G before conversion to fish population density, with our standard 6-sample (3-ping and 2-range-cell) intensity average. (B) Mean measured pressure level along the transect in Fig S5A appears with experimentally determined standard deviations for our standard 6-sample (3-ping and 2-range-cell) intensity average. (C) Expected two way transmission loss (TL) along transect in S5A for depth-averaged intensity within 40 m of the seafloor where fish shoals were observed by CFFS (Fig 2). Computed by parabolic equation-based Monte Carlo modeling (*SII*) with measured bathymetry and oceanography. The trend is dominated by two-way cylindrical spreading. Error bars show roughly 1 dB standard deviation of 40-m depth average at given ranges indicating low variation in expected 2-way TL over fish shoal depths observed in Fig 2.

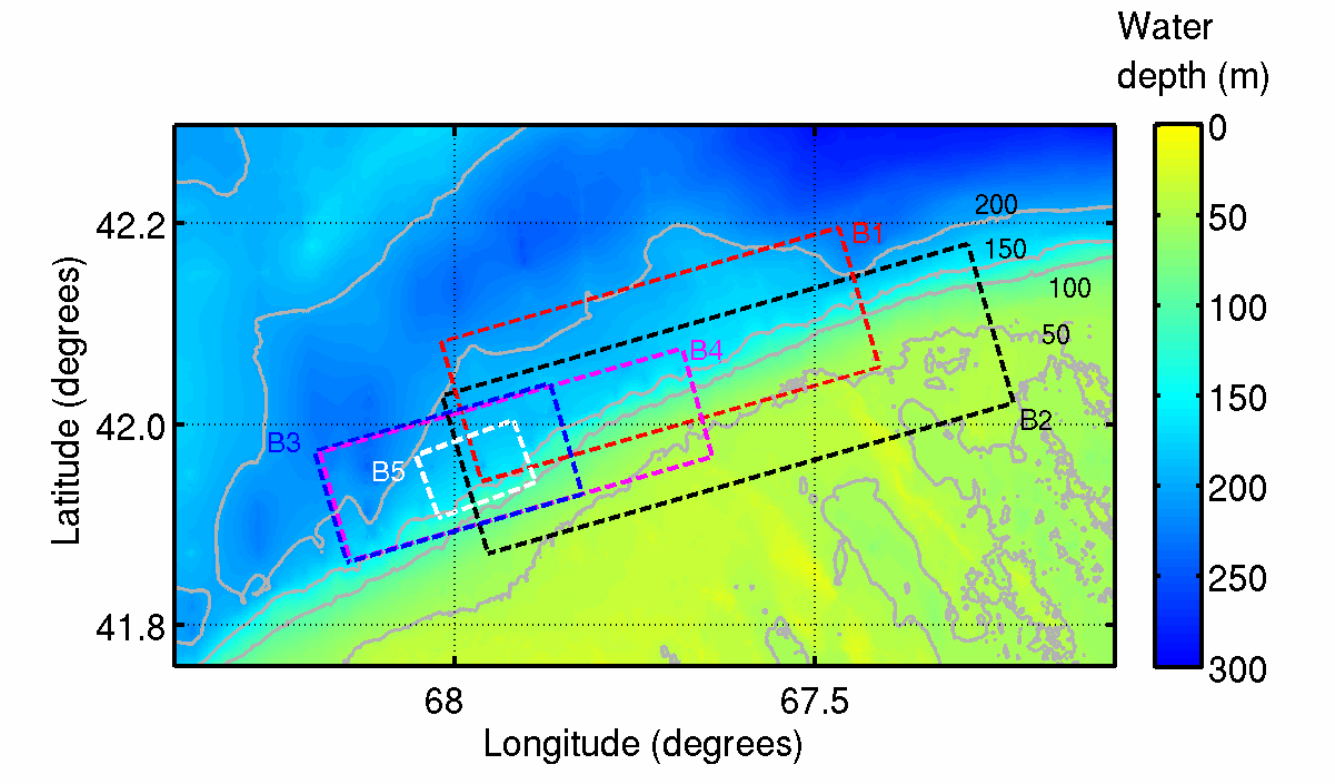

Fig S6. Georges Bank bathymetry in the region of the OAWRS images shown in Figs S1-S4. Boxes B1 and B2 are regions shown in Fig 1G-L and Fig 4A-D, respectively. Boxes B3, B4 and B5 are regions shown in Figs S1A-B, S2A-B and S4A-B respectively.

Supporting references and notes

S1.Lord Rayleigh, *The Theory of Sound* (Dover, New York, 1896), Vol. 2, Ch. 15, p. 296.

S2. J. Toner, Y. Tu, *Physical Review E.*, **59 (4)** (1998).

S3. D. V. Radakov, in *Schooling in the ecology of fish* (John Wiley & Sons, New York, 1973).

S4. P. Fréon, O. A. Misund, *Dynamics of Pelagic Fish Distribution and Behavior: Effects on Fisheries and Stock Assessment* (Fishing News Books, Oxford, 1999).

S5. O. A. Misund, A. Aglen, and E. Froenaes, *ICES J. Mar. Sci.*, **52 (1)** (1995).

S6. F. Gerlotto, M. Soria, P. Fréon, *Can. J. Fish. Aquat. Sci*. **56** (1999).

S7. T. J. Pitcher, in *Encyclopedia of Ocean Sciences*, J. H Steele, K. K. Turekian, S. A. Thorpe, Eds. (Academic Press, London, 2001), pp. 978-987.

S8. N. C. Makris, P. Ratilal, D. T. Symonds, S. Jagannathan, S. Lee, R. W. Nero, *Science*, **311**, 660-663 (2006) and Supporting Online Material.

S9. R. Urick, *Principles of Underwater Sound* (McGraw-Hill, New York, 1983).

S10. Chen, Ratilal, Makris, *J. Acoust. Soc. Am.* **118**, 3560 (2005).

S11. Andrews, Chen, Ratilal, *J. Acoust. Soc. Am.* **125**, 111 (2009).

S12. J. W. Goodman, Statistical Optics (Wiley, New York, 1985).

S13. N. C. Makris, *J. Acoust. Soc. Am*. **100**, 769 (1996).

S14. N. C. Makris, *Opt. Lett.* **20**, 2012 (1995).

S15. N. C. Makris, L. Avelino, R. Menis, *J. Acoust. Soc. Am*. **97**, 3547 (1995).

S16. P. Ratilal, Y. Lai, D. T. Symonds, L. A. Ruhlmann, J. R. Preston, E. K. Scheer, M. T. Garr, C. W. Holland, J. A. Goff, and N. C. Makris, *J. Acoust. Soc. Am.* **117**, 1977-1998 (2005).